Volume 8
Number 15
7 August 2024
Pages 3195–3466

Sustainable Energy & Fuels

Interdisciplinary research for the development of sustainable energy technologies

rsc.li/sustainable-energy

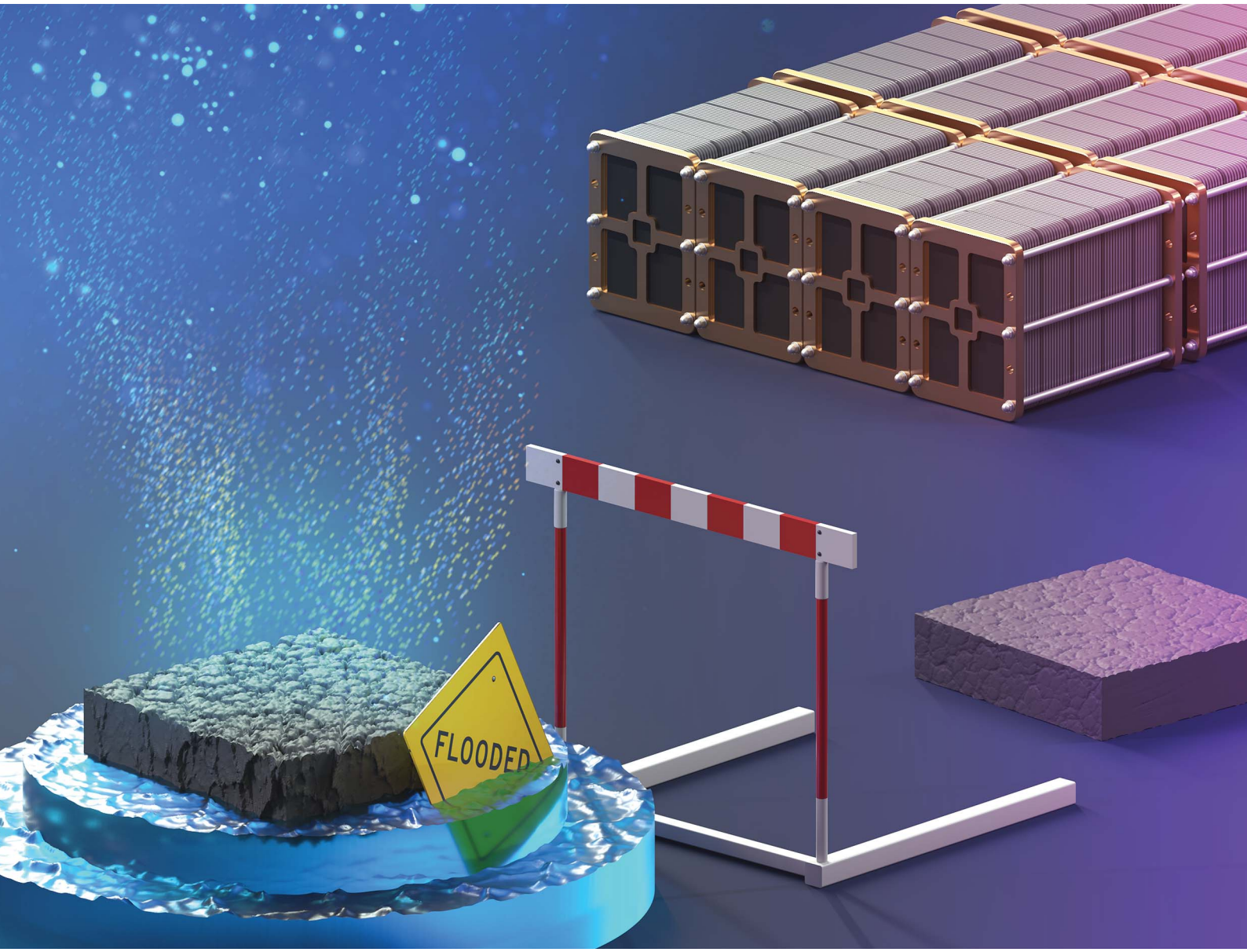

ISSN 2398-4902

ROYAL SOCIETY OF CHEMISTRY

PAPER
Jack R. Ferrell *et al.*
Carbon corrosion in low-temperature CO_2 electrolysis systems

Sustainable Energy & Fuels

ROYAL SOCIETY OF CHEMISTRY

PAPER

View Article Online
View Journal | View Issue

Check for updates

Cite this: *Sustainable Energy Fuels*, 2024, **8**, 3266

Carbon corrosion in low-temperature CO_2 electrolysis systems†

Jack R. Ferrell, ‡, III* Mathew Rasmussen ‡ and W. Wilson McNeary

Carbon corrosion has been widely documented in electrochemical systems such as fuel cells and water electrolyzers. In these systems, CO_2 is neither a reactant or a product, and CO_2 produced from carbon corrosion can be directly measured and attributed to the carbon corrosion process. In CO_2 electrolysis, the CO_2 feed masks the detection of CO_2 produced from anodic carbon corrosion, making the quantification of carbon corrosion difficult. Additionally, current CO_2 electrolysis systems operate in a different chemical environment than fuel cells and water electrolysis systems, often employing a carbonate-based anolyte. Understanding and quantifying failure modes is critical for the commercialization of CO_2 electrolysis, where a durability of multiple years is required. However, at present, many published studies employ carbon-based materials on the anode. These carbon-based anodes may corrode and deteriorate under the oxidative potentials present on the anode under normal CO_2 electrolysis operation. Carbon corrosion at the anode may also be convoluted with other common degradation mechanisms, making quantification of specific degradation pathways more challenging. Here, we have developed an *ex situ* carbon corrosion test for CO_2 electrolysis that allows for the quantification of mass loss from carbon corrosion. Using this test, significant carbon corrosion has been quantified at realistic anodic voltages experienced in operating CO_2 electrolysis cells. Based on these results, and informed from the past experiences in the development of fuel cell and water electrolysis systems, we provide a perspective on the use of carbon-based materials on the anode of CO_2 electrolysis systems. The CO_2 utilization community would benefit from rapidly transitioning away from the use of carbon-based materials on the anode of CO_2 electrolysis systems. If carbon materials are used on the anode in CO_2 electrolysis systems, it is only appropriate for short-term (<100 h) experiments.

Received 2nd May 2024
Accepted 22nd May 2024

DOI: 10.1039/d4se00594e

rsc.li/sustainable-energy

Open Access Article. Published on 31 Motsheanong 2024. Downloaded on 2024-10-01 10:24:49.
This article is licensed under a Creative Commons Attribution 3.0 Unported Licence.

1. Introduction

In recent years, it has become obvious that dramatic changes to our fossil fuel-based economy are needed to limit global warming to less than 2 °C.[1] Decarbonization of electricity generation alongside deep electrification of our current economy is the leading strategy to accomplish this goal and avoid the worst effects of climate change. However, many sectors of our economy, such as aviation, chemicals manufacturing, and marine shipping will require hydrocarbon-based feedstocks for the foreseeable future.[2] A prevailing strategy to move away from fossil-based feedstocks is the use of waste CO_2 as a carbon source. By using CO_2 that already exists within the anthropogenic carbon cycle, fuels and chemicals can be synthesized with a dramatically lower carbon footprint when CO_2 conversion is powered by renewable energy.[3] Additionally, CO_2 is available in all regions of the world, at a scale that can meet global demand for fuels and chemicals. This is advantageous to other sustainable carbon sources such as biomass, which can vary regionally and does not exist at a sufficient scale to replace all carbon-based products used today.[4]

Of the many CO_2 utilization pathways available, low-temperature CO_2 electrolysis has many advantages,[5] including the direct use of renewable electricity to drive the energy-intensive conversion of CO_2, potential for higher energy efficiency as compared to thermochemical and biochemical conversions, scalability and modularity (including the potential for smaller-scale distributed deployment as compared to the large-scale centralized facilities employed in fuel and chemical production today), and the benefit of shorter startup/shutdown times allowing for coupling with the intermittency of renewable electricity sources. Despite significant recent interest in low-temperature CO_2 electrolysis, this technology remains at a relatively low technology readiness level (TRL) of ~3–5, and advances are needed in performance (*e.g.*, increasing current density, single-pass conversion, product selectivity, and lowering cell voltage), durability, scaling up to larger electrolyzer designs, and scaling out to larger electrolyzer stack sizes.[6–8]

National Renewable Energy Laboratory, 15013 Denver W Pkwy, Golden, CO 80401, USA. E-mail: jack.ferrell@nrel.gov

† Electronic supplementary information (ESI) available. See DOI: https://doi.org/10.1039/d4se00594e

‡ J. Ferrell and M. Rasmussen contributed equally to this work.

This journal is © The Royal Society of Chemistry 2024

Open Access Article. Published on 31 Motsheanong 2024. Downloaded on 2024-10-01 10:24:49.
This article is licensed under a Creative Commons Attribution 3.0 Unported Licence.

Several electrolyzer designs have been studied over the years for electrochemical CO_2 reduction. Many initial, fundamental studies utilized liquid phase batch type reactors (*e.g.*, H-cells), but due to a variety of issues, including significant mass transport limitations, it is widely understood that H-cells are not practical for industrial-scale deployment.[9] Continuous flow electrolyzers are needed to achieve relevant current densities for commercial adoption.[6,9,10]

Most continuous flow CO_2 electrolyzer designs can be broadly classified into three categories: membrane electrode assemblies (MEAs), microfluidic reactors, and solid oxide electrolysis cells (SOECs).[9] SOECs utilize an ion-conducting solid oxide material, typically yttria-stabilized zirconia, and operate at high temperatures (>600 °C) with gas-phase CO_2 diffusing and reacting directly on the cathode to form gas-phase products.[11,12] Microfluidic reactors and MEAs share many common characteristics, including the use of gas diffusion electrodes (GDEs). In essence, GDEs are porous electrodes that allow for diffusion of gas phase CO_2 to reaction sites. GDEs are usually designed with two main components: a nanoparticle catalyst layer, and a highly porous gas diffusion layer (GDL) support, which is often composed of carbon paper and a carbon-based microporous layer (MPL).[13,14] The most common microfluidic reactor architecture relies on two GDEs separated by a flowing electrolyte solution, with gas-phase CO_2 being fed continuously to the cathode GDE.[15] MEAs, on the other hand, typically utilize two GDEs separated by an ion-exchange membrane, which may consist of a proton exchange membrane (PEM) or an alkaline exchange membrane (AEM). In one of the most common MEA configurations, CO_2 is delivered to the cathode GDE (often as a humidified gas) where it diffuses to the catalyst layer and is reduced to the desired product, while pure water or an anolyte solution is fed to the anode GDE as a source of electrons through the oxygen evolution reaction (OER).[16,17] Shown in Fig. 1 is a common architecture for MEA based electrolyzers.

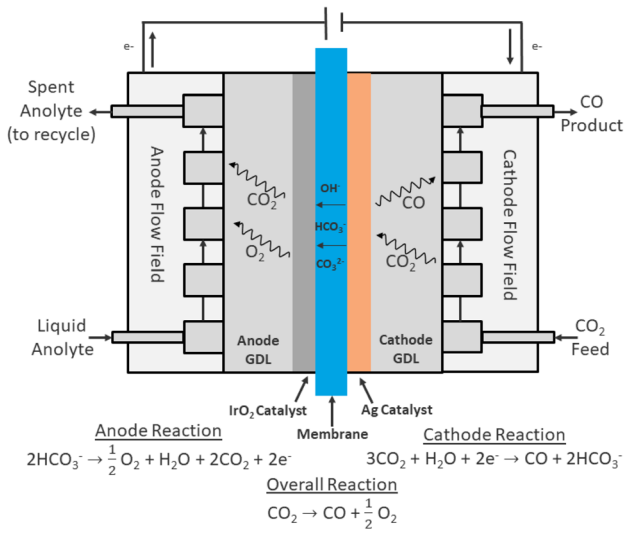

Fig. 1 Cross section of a common MEA used in CO_2 electrolysis. Here, an AEM membrane transports anions from cathode to anode, an Ag cathode catalyst produces CO, and the IrO_2 anode catalyst evolves oxygen from the OER reaction and CO_2 is produced from carbonate crossover through the membrane.

Proving the long-term durability these low-temperature CO_2 electrolysis MEAs remains a critical challenge for commercialization of this technology. The vast majority of published studies on CO_2 MEAs do not report durability data; those that do typically report a durability of <100 hours.[18] However, techno-economic analyses that estimate the minimum selling price of products from CO_2 electrolysis typically assume an MEA lifetime of >4 years.[6,19] This large discrepancy in MEA lifetime must be met by targeted research efforts focused on understanding and mitigating failure modes.[20] Numerous failure modes exist, including membrane failure, MEA delamination, salt precipitation, catalyst degradation, poor water management, binder degradation, and carbon corrosion.[21]

Carbon corrosion, in particular, has been identified as a persistent problem for all types of low-temperature electrochemical devices, including fuel cells and electrolyzers. In proton exchange membrane fuel cells (PEMFCs), carbon corrosion occurs rapidly during voltage excursions caused by fuel starvation, poor flow distribution, gas blockages, sudden current changes, and startup/shutdown processes.[22,23] The PEMFC community has studied the effects of these voltage excursions through a variety of different carbon corrosion accelerated stress tests (ASTs), including voltage holds[24] as well as voltage cycling.[25] Overall, the PEMFC community has documented multiple degradation pathways resulting from carbon corrosion, including reduced catalyst layer thickness and porosity, catalyst agglomeration, reduction in electrochemical surface area (ECSA),[26] water flooding, reduced capillary pressure, increased electrical resistance,[27] and loss of mechanical strength.[28] Anion exchange membrane fuel cells (AEMFCs) have shown performance and durability improvements in recent years, but still suffer from many of the same adverse effects of carbon corrosion observed in PEMFCs.[29] Water electrolyzers, on the other hand, experience higher anodic voltages for longer periods of time than fuel cells, due to the high onset potential (1.23 V *vs.* SHE in acidic media) for the anode reaction – the oxygen evolution reaction (OER). As a result, strict material requirements have been put in place for these electrolysis systems. Alkaline water electrolysis (AWE) systems have employed nickel and stainless-steel materials for the past 100 years.[30] Similarly, PEM water electrolyzers rely on materials that are highly resistant to corrosion, such as platinum group metal catalysts, titanium bipolar plates,[31] and various types of non-carbon porous transport layers (PTLs).[32]

CO_2 electrolyzers rely on the same electrochemical reaction on the anode (*i.e.*, OER) as water electrolyzers, so similar anodic material requirements are expected. However, at present, many published studies in CO_2 electrolysis employ carbon-based gas diffusion media on the anode.[33–43] In contrast to the research literature, most industrial CO_2 electrolysis startups (Det Norske Veritas,[10,44] Mantra Energy,[10,45,46] Dioxide Materials,[43,47,48] Siemens/Evonik,[49–53] Liquid Light/Avantium,[54–58] and Twelve/Opus 12 [59–63]) have already switched to alternative materials on the anode, such as stainless steel or TiO_2. This dichotomy represents a gap between fundamental research and practical

Open Access Article. Published on 31 Motsheanong 2024. Downloaded on 2024-10-01 10:24:49.
This article is licensed under a Creative Commons Attribution 3.0 Unported Licence.

application that should be addressed with focused research efforts. Thorough characterization of carbon corrosion under conditions relevant to CO_2 electrolysis is needed to understand the impact of carbon corrosion on electrolyzer lifetime and to identify compatible anode materials.

Several challenges exist for quantifying and mitigating carbon corrosion in CO_2 electrolyzers. For one, long-term durability testing is time-consuming and resource-intensive, and as a result, may be infeasible for many research institutions. ASTs and accelerated durability tests (ADTs) are needed to rapidly screen the stability of materials and components under relevant conditions. Some ADT and AST protocols have already been developed for other low-temperature electrochemical devices such as proton exchange membrane fuel cells (PEMFCs)[64] and water electrolyzers,[65] and these learnings can be leveraged to quickly develop ADT/AST tests relevant to CO_2 electrolysis.[18] Another challenge with measuring carbon corrosion in CO_2 electrolyzers is related to the presence of alkaline media. Many CO_2 electrolysis systems employ an alkaline exchange membrane (AEM) to improve faradaic efficiency, but carbon exhibits low thermodynamic stability in alkaline conditions. Pourbaix diagrams show that carbon is thermodynamically stable only between −0.23 and 0.00 V (*vs.* SHE) at pH = 7,[66] and the kinetics for carbon corrosion accelerate in alkaline environments due to OH-anions being efficient nucleophiles. Quantification of CO_2 as a marker for carbon corrosion in basic solutions is challenging, because alkaline electrolytes tend to convert gaseous CO_2 into solvated (bi) carbonate anions, which cannot be detected by gas chromatography (GC).[67] Additionally, quantification of CO_2 in operating AEM MEAs is particularly difficult due to the presence of CO_2 at both the cathode (as a feed gas) and at the anode (from CO_2 crossover), thereby masking the CO_2 that is produced from the carbon corrosion process. As a result of these factors, relatively few studies have been published on the mechanism and rate of carbon corrosion in alkaline environments, such as for AEM-based CO_2 electrolyzers.[67]

In this work, we report on the development of a simple, accelerated *ex situ* test to study anodic carbon corrosion for CO_2 electrolysis. This *ex situ* test can easily be operated as an AST or a long-term durability test by adjusting the oxidative voltage at the working electrode. Additionally, this test avoids the challenges with quantifying carbon corrosion in an operating MEA by removing the CO_2-fed cathode from the system, thereby minimizing convolution of the CO_2 corrosion product. Finally, by employing multiple quantification techniques (mass loss, CO_2 evolved, and total current passed), we are better able to measure and verify the rate of carbon corrosion during each experiment.[26]

2. Experimental

2.1. Carbon corrosion testing

Ex situ carbon corrosion experiments were conducted using a three-electrode setup in a Gamry Eurocell. Corrosion samples were cut from a carbon paper-based gas diffusion layer (AvCarb GDS 5130, Sigracet 39BB, or Toray Paper 120 with MPL) an IrO_2-coated carbon paper-based gas diffusion electrode (Dioxide Materials, CO_2 Anode), or a non-carbon porous transport layer (Titanium Fiber Felt 0.2–0.3 mm, Fuel Cell Store) depending on the experiment. Samples were cut consistently using a rigid, 3-D printed stencil to a size of 5 cm × 1.9 cm (9.5 cm^2 total area) with a 2 cm × 0.9 cm tab on the end for clipping to the potentiostat (BioLogic SP-300). The threaded sample rod (Gamry Eurocell Kit) was modified with a toothless alligator clip for clamping onto the corrosion sample. A saturated Ag/AgCl electrode (36% w/w, Gamry) was used as the reference and was introduced to the cell solution through a bridge tube. The counter electrode for each experiment was a Pt wire with Pt mesh. The electrochemical cell was filled with an electrolyte solution containing either potassium bicarbonate ($KHCO_3$) or potassium phosphate (KH_2PO_4/K_2HPO_4) solution, depending on the experiment. The concentration and pH of the potassium phosphate electrolyte was matched to the concentration and pH of the potassium bicarbonate electrolyte, typically 5 mM and pH ≈ 8. N_2 was continuously bubbled through the airtight cell with a fritted bubbler at 15 sccm, pushing gas-phase products to the downstream micro gas chromatograph (Agilent 490 μGC). Each experiment was conducted in potentiostatic-mode, holding the corrosion sample at a given oxidative potential for a period of time long enough to detect changes in the sample mass. All potentials are reported *versus* the Ag/AgCl reference electrode.

2.2. Electrode mass loss calculations

Mass loss through carbon corrosion was quantified through several methods. The actual net mass loss was determined by weighing the corrosion sample before and after each experiment on a mass balance. Samples were rinsed thoroughly with DI water and dried in an oven at 110 °C for 30 minutes before each weight measurement.

Estimates for the expected mass loss during each experiment were calculated based on measurements at the potentiostat and gas chromatograph (GC). Gas phase products were carried to the GC by a continuous flow of 15 sccm N_2 through the cell. The only gas-phase carbon corrosion product detected was CO_2 (*i.e.*, no CO was detected by the GC). This is consistent with the unfavourable thermodynamics for carbon oxidation to CO compared to CO_2.[68,69] The total mass loss was calculated by summing the CO_2 detected during each GC injection according to the following equation:

$$\text{GC mass loss estimate} = \sum C_{CO_2} \times \dot{n}_{N_2} \times \Delta t \times \frac{M_C}{M_{CO_2}}$$

where C_{CO_2} represents the molar CO_2 concentration for a particular GC injection, $\dot{n}_{N_2}$ represents the molar flowrate of N_2 through the cell, Δt represents the time between GC injections, and M_C/M_{CO_2} represent the ratio between the molar masses of carbon and carbon dioxide.

Mass loss *via* carbon corrosion was also calculated based on the current measured at the potentiostat throughout the experiment according to the following equation:

$$\text{Potentiostat mass loss estimate} = \sum \frac{i_{PS}}{F} \times \frac{1\ \text{mol}\ CO_2}{4\ \text{mol}\ e^-} \times \Delta t \times \text{FE}$$

 This journal is © The Royal Society of Chemistry 2024

Open Access Article. Published on 31 Motsheanong 2024. Downloaded on 2024-10-01 10:24:49.
This article is licensed under a Creative Commons Attribution 3.0 Unported Licence.

where i_{PS} represents the current measured by the potentiostat at a given timepoint in amps, F is Faraday's constant (96 485.3 C mol^{-1}), Δt represents the time between potentiostat measurements, and FE is the faradaic efficiency (FE) for carbon corrosion to CO_2. For carbon-based GDL samples, the faradaic efficiency for carbon corrosion to CO_2 was assumed to be unity. No gas-phase corrosion products other than CO_2 were detected during any experiment, and no oxygen was detected, indicating that the OER reaction was negligible for GDLs without a catalyst. For experiments involving carbon-based GDLs with an IrO_2 catalyst, the FE value was calculated based on the molar ratio of $CO_2 : O_2$ detected by the GC near the end of the experiment, due to the substantial rate of OER.

2.3. Corrosion sample characterization

Physicochemical changes in the electrode from carbon corrosion were visually analysed through scanning electron microscopy (SEM) using an FEI Quanta 400 FEG instrument under high vacuum operating with the Everhart Thorney Detector. Samples were prepared for imaging by mounting on aluminum stubs using carbon tape with conductive silver paint applied to the sides to reduce sample charging. Imaging was performed at beam accelerating voltages from 20 to 30 kV. An EDAX element energy dispersive spectroscopy (EDS) system was utilized to create spectral maps of the front and back of electrode samples. All EDS spectral maps shown in this paper (including the ESI†) were corrected in PowerPoint with +40% saturation and −40% contrast to make the coloring more apparent. The Elements software was utilized to determine approximate weight percentages of each element detected in each spectral map. These weight percentages were utilized to calculate ratios of certain species (such as a C : F ratio) for comparison between different samples.

Changes in the elemental composition of electrodes and electrolytes were determined through inductively coupled plasma optical emission spectroscopy (ICP-OES) using an Agilent 5110 ICP-OES. Solid samples were digested in 4 mL of aqua regia solution (3 : 1 – $HCl : HNO_3$). Elements quantified included iridium, potassium, phosphorus, and copper.

3. Results

The rate of carbon corrosion was tested over a variety of oxidative voltages (1.0–2.0 V *vs.* Ag/AgCl) for a commercial, carbon-based GDL from AvCarb. The AvCarb GDL is comprised of a carbon fiber layer (CFL) backbone, a polytetrafluoroethylene (PTFE) treatment, and a MPL on one side.

Shown in Fig. 2 is a semi-log plot of the current density (as measured by the potentiostat) and CO_2 evolved (as measured by the GC) over the course of a series of corrosion tests in phosphate electrolyte. These two measurements represent different strategies for quantifying the rate of carbon corrosion. Lower voltage tests were held for longer periods of time to obtain measurable mass losses: 24 h at 2.0 V *vs.* Ag/AgCl (Fig. 2A), 72 h at 1.6 V *vs.* Ag/AgCl (Fig. 2B), 128 h at 1.2 V *vs.* Ag/AgCl (Fig. 2C), and roughly 1300 h at 1.0 V *vs.* Ag/AgCl (Fig. 2D). At the two lower corrosion potentials, 1.2 V and 1.0 V *vs.* Ag/AgCl, the rate of CO_2 production was below the detection limits of the GC, so no CO_2 flowrate is displayed for those tests.

The corrosion current measured the potentiostat varied by nearly three orders of magnitude between the highest (2.0 V, Fig. 2A) and lowest voltages (1.0 V, Fig. 2D) explored in this study. Generally, the rate of carbon corrosion increased over the course of each experiment. This may be due to carbon corrosion creating imperfections in the electrode surface, thereby increasing the surface area in contact with the electrolyte. For experiments where CO_2 was detectable, the CO_2 flowrate gradually increased to a steady-state value at the beginning of the experiment. This transient behavior was likely due to the equilibrium between CO_2 and bicarbonate in basic solutions:

$$CO_2(g) + OH^-(aq) \rightleftharpoons HCO_3^-(aq)$$

The normalized mass loss per day calculated for the GDLs in these experiments are reported in Table 1. In general, the mass loss exhibited an exponential relationship with the oxidative potential with 0.1%, 0.3%, 2.8%, and 10.9% of the initial GDLs mass being lost per day at 1.0 V, 1.2 V, 1.6 V, and 2.0 V *vs.* Ag/AgCl, respectively. Clearly, for any electrochemical system using carbon-based GDLs, it is essential to minimize the oxidative potential experienced at the anode to avoid the irreversible loss of carbon by the carbon corrosion process.

Typically, potassium bicarbonate ($KHCO_3$) electrolyte is utilized for operation of AEM MEA electrolyzers, rather than the potassium phosphate (KH_2PO_4/K_2HPO_4) utilized in this study. However, bicarbonate electrolyte makes quantification of carbon corrosion more difficult, due to the potential decomposition of the bicarbonate into CO_2(g), thereby convoluting the corrosion-based CO_2(g) signal detected by the GC. This issue can be avoided by using a similar electrolyte, such as potassium phosphate, which does not contain carbon as a potential source of CO_2 during the experiment. To determine the validity of corrosion experiments conducted in phosphate electrolyte, a series of corrosion tests were conducted in potassium bicarbonate solution (5 mM) and compared to identical tests in potassium phosphate solution (5 mM, pH = 8) at 2.0 V *vs.* Ag/AgCl for 24 h (Fig. S2A†) and 1.6 V *vs.* Ag/AgCl for 72 h (Fig. S2B†). The potentiostat, GC, and mass balance estimates of mass loss were similar in both electrolyte solutions, but the GC-estimated mass loss was slightly higher for the bicarbonate electrolyte compared to the phosphate electrolyte at both 1.6 and 2.0 V *vs.* Ag/AgCl. This result was expected and was likely due to convolution of CO_2 produced through carbon corrosion and CO_2 produced through decomposition of $KHCO_3$. The normalized daily mass loss was similar for both electrolytes (Table 1); phosphate solution gave 10.9% mass loss per day at 2.0 V and 2.8% mass loss per day at 1.6 V, while bicarbonate solution gave 9.1% mass loss per day at 2.0 V and 2.9% mass loss per day at 1.6 V. Overall, these results demonstrate that phosphate and bicarbonate electrolytes exhibit similar rates of carbon corrosion, but the phosphate electrolyte allows for more detailed corrosion measurements *via* reliable detection of CO_2 produced from the carbon corrosion process.

Open Access Article. Published on 31 Motsheanong 2024. Downloaded on 2024-10-01 10:24:49.
This article is licensed under a Creative Commons Attribution 3.0 Unported Licence.

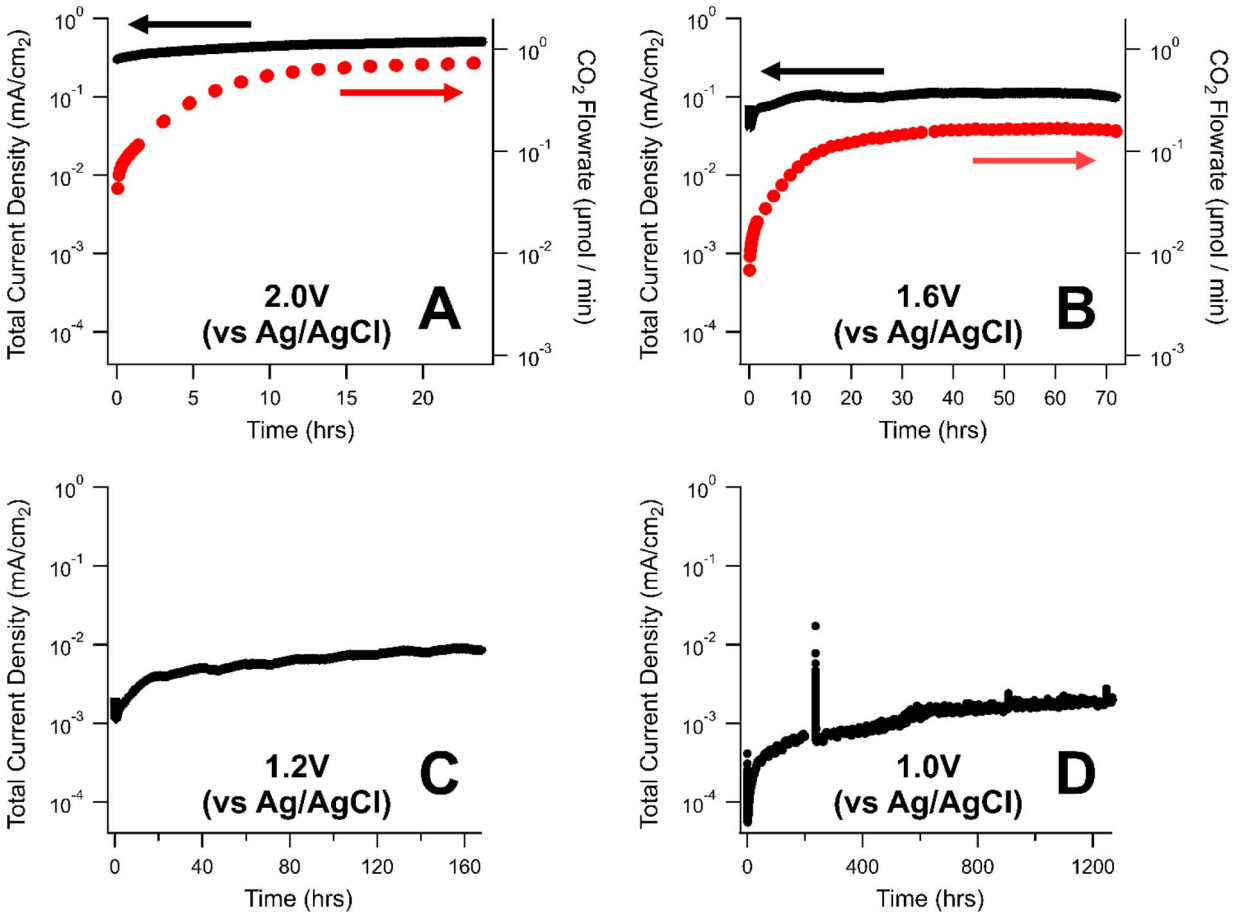

Fig. 2 Carbon corrosion rates of a GDL held at oxidative potentials of 2.0 V (A), 1.6 V (B), 1.2 V (C), and 1.0 V (D) with respect to a saturated Ag/AgCl reference electrode. Electrolyte was a phosphate solution (5 mM, pH = 8). Black markers represent the current density (measured by the potentiostat) while red markers represent the flowrate of CO_2 evolved from the GDL (calculated from the online GC).

Another control experiment in 5 mM $KHCO_3$ was conducted with Pt mesh as the working electrode rather than a carbon-based GDL to determine whether the bicarbonate solution was electrochemically active. This experiment generated measurable amounts of CO_2, particularly at highly oxidative potentials (*i.e.*, 2.0 V *vs.* Ag/AgCl). This experiment highlighted the benefit of using electrolytes other than bicarbonate when quantifying and characterizing carbon corrosion.

The replicability of this corrosion testing protocol was investigated *via* a triplicate experiment in phosphate electrolyte (5 mM, pH = 8) at 2.0 V *vs.* Ag/AgCl for 24 h using smaller, hand-cut 7.5 cm^2 AvcCarb GDL electrodes (Fig. S1†). Electrodes were

Table 1 Compiled carbon corrosion test results for an AvCarb GDS 5130 GDL in phosphate and bicarbonate electrolyte solutions at 1.0–2.0 V (*vs.* Ag/AgCl)

					Mass loss (mg)			
Voltage (*vs.* Ag/AgCl)	Voltage (*vs.* SHE)	Corrosion time (h)	Electrolyte type	Initial electrode mass (mg)	Potentiostat estimate[a]	GC estimate[b]	Mass balance measurement[c]	% Mass loss per day[c]
2.0	2.197	24	Phosphate	83.2	11.3	10.0	9.1	10.9%
			$KHCO_3$	82.6	11.6	11.2	7.5	9.1%
1.6	1.797	72	Phosphate	82.1	7.9	7.0	7.0	2.8%
			$KHCO_3$	81.9	10.7	10.0	7.1	2.9%
1.2	1.397	168	Phosphate	82.1	1.1	—	1.5	0.3%
1.0	1.197	1293	Phosphate	80.5	1.7	—	2.2	0.1%

[a] Estimated from the potentiostat-measured current. [b] Estimated from the GC-measured CO_2 flowrate. [c] Reported value comes from mass balance measurements before and after corrosion experiment.

 This journal is © The Royal Society of Chemistry 2024

Open Access Article. Published on 31 Motsheanong 2024. Downloaded on 2024-10-01 10:24:49.
This article is licensed under a Creative Commons Attribution 3.0 Unported Licence.

weighed before and after each experiment to determine the relative weight loss due to carbon corrosion. The relative mass loss as a percentage of the initial GDL mass was calculated as 12.37% ± 0.04% for this triplicate study. This low standard deviation demonstrates the high degree of reproducibility for the corrosion tests utilized in this study.

SEM-EDS images of a fresh and corroded GDL were collected to obtain a visual representation of the effects of carbon corrosion (Fig. 3). The corroded electrode was exposed to harsh, accelerated corrosion conditions at 2.0 V *vs.* Ag/AgCl for 48 h in bicarbonate electrolyte. The measured mass loss for the GDL during this experiment was 11.0 mg, or 19.7% of its initial mass.

After corrosion, the CFL (Fig. 3B) showed clear signs of degradation, with the interstitial region between individual fibers exhibiting significant erosion. Evidence for fracturing of carbon fibers can also be seen within the eroded region in the middle-left of Fig. 3B. Indications of corrosion on the MPL (Fig. 3D) were more difficult to discern through SEM, although the corroded sample appeared to exhibit some pockmarking. Very similar SEM results have been reported in PEMFCs for the CFL and the MPL.[27] EDS elemental mapping of the MPL (Fig. 3E and F), however, revealed dramatic signs of carbon corrosion. Before corrosion, the SEM-EDS map is dominated by red (carbon) pixels, whereas after corrosion, the EDS map displays a much higher proportion of orange (fluorine) pixels. In fact, the weight-based ratio of C : F detected in the EDS maps dropped from 3.0 : 1.0 before corrosion to 1.1 : 1.0 after corrosion. This change is caused by carbon particles oxidizing into the gas phase as CO_2, thereby revealing the underlying fluorine-based PTFE. The post-corrosion sample also exhibited detectable amounts of oxygen and potassium in the EDS map. The presence of oxygen in the sample after corrosion may indicate that surface oxide intermediates were formed on the way to complete oxidation to CO_2. The potassium detected in the sample was likely due to precipitation of the $KHCO_3$ electrolyte on the MPL. Similar changes were seen in the EDS map of the CFL, as shown in Fig. S3,† with the weight-based ratio of C : F dropping from 3.0 : 1.0 before corrosion to 1.6 : 1.0 after corrosion.

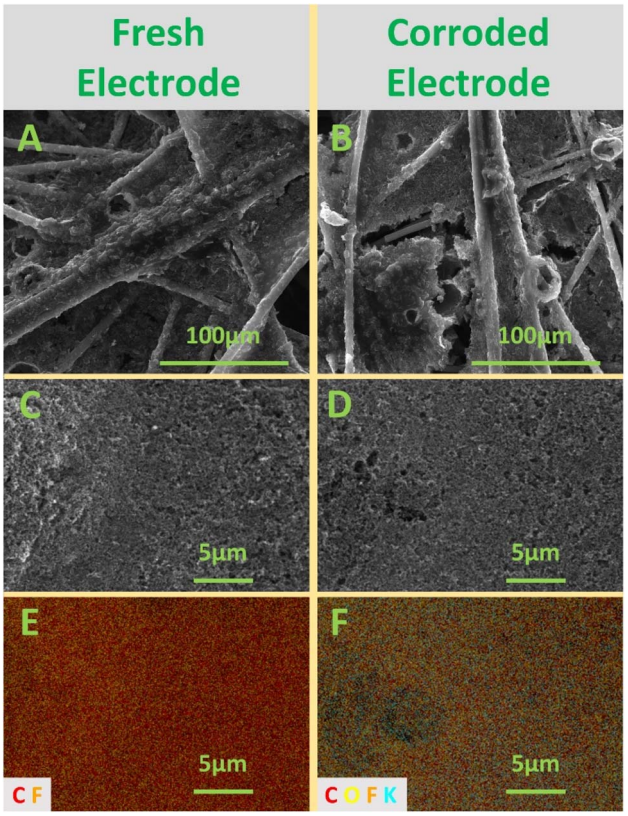

Fig. 3 SEM images and EDS mapping for a fresh (A, C and E) and corroded (B, D and F) carbon-based GDL. Corrosion conditions were 48 h at 2.0 V *vs.* Ag/AgCl in bicarbonate electrolyte solution. SEM images of the carbon fiber layer (A and B) are displayed. SEM images of the microporous layer (C and D) are displayed along with the corresponding EDS map (E and F) for those images.

Another series of experiments were conducted on commercially available GDLs from various manufacturers to determine whether any specific GDL properties are related to the rate of carbon corrosion. The AvCarb GDS 5130 results (Fig. 1 and 2) were compared to Sigracet 39BB, Toray Paper TGP-H-120 w/ MPL, and a TiO_2 Fiber Felt all purchased from the Fuel Cell Store. Relevant properties for each anode material are compiled in Table S1.† Triplicate corrosion tests were performed for each GDL in potassium phosphate solution (5 mM, pH = 8) at 2.0 V *vs.* Ag/AgCl for 24 h. The TiO_2 Fiber Felt anode was tested only once under the same conditions. Shown in Table 2 are the averaged results from these experiments.

The various GDLs tested for carbon corrosion exhibited a range of physical properties, including different area densities and PTFE loadings (Table S1†). Regardless, the measured mass loss from corrosion at 2.0 V for 24 h was similar for all GDLs (within error) regardless of manufacturer. The overall measured % mass loss per day (Table 2) for each GDL was inversely correlated with the area density (Table S1†) and initial electrode mass. This result suggests that electrodes with a greater thickness and area density may last longer in corrosive environments, simply because there is a larger amount of carbonaceous material that must be oxidized before the anode fails. The impact of GDL properties on electrolyzer performance has only recently gained attention for the CO_2 reduction reaction.[70] On the cathode, studies have found that thicker MPLs and GDLs help suppress electrolyte flooding,[71] maximize selectivity to the desired reduction product (particularly at high current densities),[70,71] and improve long-term electrolyzer performance.[70] On the anode, Schwartz *et al.* found that thicker GDLs exhibited superior performance and attributed this to the their ability to retain water within the membrane and catalyst layers.[72] Further research in this area is needed to develop structure–performance relationships for GDLs and rationally design anodes for CO_2 electrolysis. It is possible that carbon-based anode GDLs with reasonable lifetimes could be developed in the future, but they are not currently on the market today.

Metal-based diffusion layers are widely utilized on the anode for water electrolyzers[73] and represent an interesting alternative to carbon-based anode GDLs in CO_2 electrolysis. Titanium,[73–76] stainless-steel,[77,78] and nickel-based[73,79–81] materials have been

Open Access Article. Published on 31 Motsheanong 2024. Downloaded on 2024-10-01 10:24:49.
This article is licensed under a Creative Commons Attribution 3.0 Unported Licence.

Table 2 Comparison of carbon corrosion test results for various anode materials conducted in phosphate electrolyte solution at 2.0 V (*vs.* Ag/AgCl)

				Mass loss (mg)				
Anode material	Voltage *vs.* Ag/AgCl	Corrosion time (h)	Electrolyte type	Initial electrode mass (mg)	Potentiostat estimate[a]	GC estimate[b]	Mass balance measurement[c]	% mass loss per day[c]
AvCarb GDS 5130	2.0	24	Phosphate	65 ± 5	12 ± 2	11	8 ± 1	12.37 ± 0.04%
Sigracet 39BB	2.0	24	Phosphate	105 ± 1	18 ± 5	15 ± 4	11 ± 4	10 ± 4%
Toray paper (TGP-H-120 w/MPL)	2.0	24	Phosphate	286 ± 5	22 ± 12	18 ± 10	12 ± 6	4 ± 2%
Titanium fiber felt	2.0	24	Phosphate	563.5	1	0	−1	0%

[a] Estimated from the potentiostat-measured current. [b] Estimated from the GC-measured CO_2 flowrate. [c] Reported value comes from mass balance measurements before and after corrosion experiment.

studied as anode materials, depending on the pH and environment at the anode. Titanium-based PTLs are the most common diffusion media for polymer electrolyte membrane water electrolyzers,[77] so we briefly explored the corrosion behavior of a titanium fiber felt. The Ti fiber felt exhibited no measurable mass loss from corrosion after exposure to the same conditions (2.0 V *vs.* Ag/AgCl for 24 h) as the various carbon-based GDLs (Table 2). This result does not suggest that Ti-based PTLs are strictly superior to carbon-based GDLs but does demonstrate that they are mechanically and structurally resistant to corrosion even at high oxidative voltages. However, utilization of Ti on the anode comes with a unique set of challenges. For example, Ti-based materials are significantly more expensive than carbon or stainless-steel components.[77,78] Additionally, exposure of Ti to anodic voltages encourages the rapid growth of an insulating TiO_2 layer on the surface.[77,82] More research in this area is needed to determine the suitability of various metal PTLs as anode diffusion layers in CO_2 electrolyzers.

While the above experiments were performed on catalyst-free GDLs, AEM CO_2 electrolyzers include an OER catalyst layer on the anode to facilitate the generation of electrons at low oxidative voltages. IrO_x-based electrocatalysts are the most commonly used OER catalyst due to their high activity and stability.[83,84]

IrO_x-based catalysts have also been investigated in the PEMFC literature to limit the effects of carbon corrosion during extreme events such as startup/shutdown or anode fuel starvation.[68,69] Typically, PEMFCs employ Pt-based catalysts on both the cathode (oxygen reduction reaction) and the anode (hydrogen oxidation reaction).[85] However, when H_2 fuel starvation occurs, the anodic hydrogen oxidation reaction is halted and replaced with water electrolysis and carbon corrosion. In response, the anode swings to high oxidative potentials to supply sufficient protons and electrons to maintain operation of the cell at a given current density.[22,23] At these elevated oxidative potentials, carbon-based GDLs corrode and fail rapidly. Some groups have developed "reversal tolerant anodes" (RTAs) to combat this degradation pathway, primarily by adding an OER catalyst, such as IrO_x, to the anode.[22,23,86–88] During fuel starvation events, these RTAs provide an alternative reaction pathway for generating electrons and protons through OER at lower oxidative voltages. While carbon corrosion still occurs, the rate is minimized due to the lower oxidative potential experienced by the GDL.

Despite the popularity of IrO_x as an OER catalyst, the effect of IrO_x on the kinetics of carbon corrosion is not well understood. Other noble metal electrocatalysts, such as Pt, have been shown to accelerate the rate of carbon corrosion compared to catalyst-free GDLs under a given set of conditions.[67,68,89–91] In contrast, IrO_x-coated GDLs have been shown to limit carbon corrosion during operando PEMFC cell operation.[22,23,86–88] However, the corrosion resistance imparted by IrO_x comes about by removing the external driving force of the corrosion reaction (the oxidative potential), not necessarily by affecting the kinetics or mechanism of the reaction itself. More fundamental studies, including cyclic voltammetry, constant potential corrosion experiments, and other tests performed for Pt-based electrocatalysts, are needed to fully characterize the effect of IrO_x-based catalysts on carbon corrosion in electrochemical devices.

In this work, we explored the effect of an OER catalyst layer on the rate of carbon corrosion using a Dioxide Materials IrO_2-coated carbon-based GDL.[34] Experiments were conducted in phosphate electrolyte solution at 2.0 V for 72 hours (Fig. 4A) and 1.6 V for 168 hours (Fig. 4B) and compared to corrosion tests performed on catalyst-free GDLs. The catalyst-coated GDLs were held under corrosive conditions for longer periods of time than the catalyst-free GDLs to obtain measurable mass losses.

At both potentials (1.6 V and 2.0 V), the IrO_2-coated GDLs generated higher current densities than the catalyst-free GDL, due to the enhanced OER kinetics (Fig. 4). Despite the increase in total current density, catalyst-coated GDLs also exhibited lower rates of CO_2 generation *via* carbon corrosion than the catalyst-free GDLs. This result suggests that the presence of the catalyst layer assists in suppressing the rate of carbon corrosion under a given set of conditions. This conclusion could be convoluted by the fact that the two samples utilized two different carbon-based GDLs – the catalyst-free GDL was an AvCarb GDS 5130 while the IrO_2-coated GDL was supported on Sigracet 35 BC. However, our corrosion tests of catalyst-free AvCarb GDS 5130 and catalyst-free Sigracet 39BB (the most similar commercially available substitute for Sigracet 35 BC)

 This journal is © The Royal Society of Chemistry 2024

Open Access Article. Published on 31 Motsheanong 2024. Downloaded on 2024-10-01 10:24:49.
This article is licensed under a Creative Commons Attribution 3.0 Unported Licence.

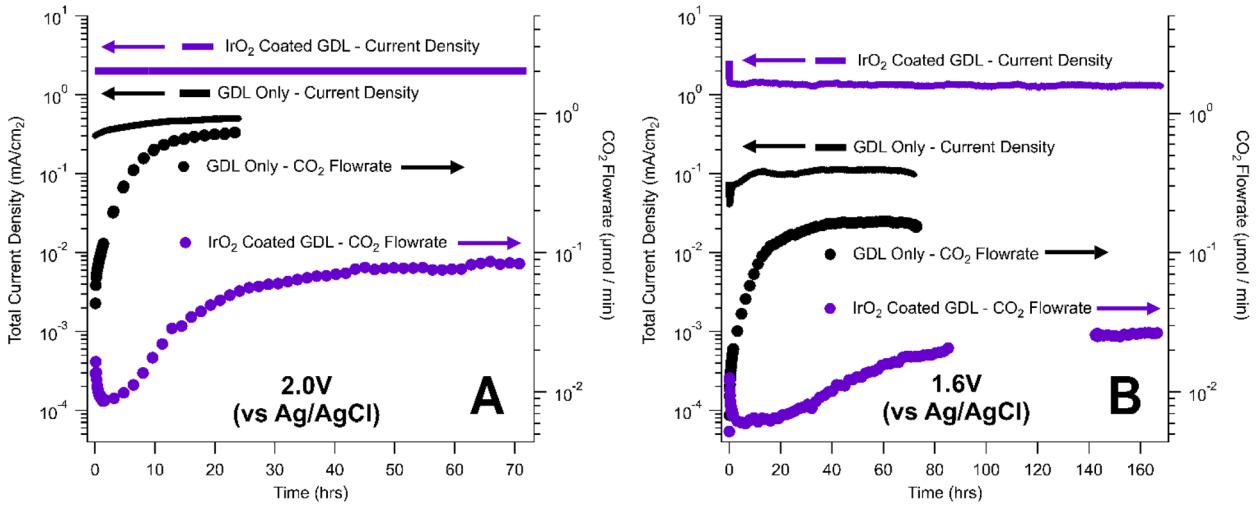

Fig. 4 Comparison of carbon corrosion rates for an IrO_2-coated GDL (purple) and AvCarb GDS 5130 GDL with no catalyst layer (black). Current density (lines, left axis) and CO_2 evolved (dots, right axis) are plotted against time for experiments held at (A) 2.0 V and (B) 1.6 V *vs.* Ag/AgCl for 24 h.

showed little or no difference between the overall rate of carbon corrosion for these two GDLs (Table 2). Perhaps more importantly, the IrO_2-coated GDL from Dioxide Materials was synthesized by spray coating an IrO_2 ink with a PTFE binder.[34] The presence of an additional PTFE layer on the MPL could enhance the corrosion resistance of the IrO_2-coated GDL compared to the native GDL. Overall, IrO_x-based catalyst layers appear to enhance the corrosion resistance of carbon-based GDLs under oxidative conditions, but the source of this corrosion resistance is currently unclear. Further fundamental research and controls are needed to determine the role of each component of the catalyst layer in suppressing carbon corrosion, thereby enabling the design of better corrosion resistant GDLs in CO_2 electrolysis and other electrochemical applications.

The measured and estimated mass losses during corrosion of the IrO_2-coated electrodes are displayed in Table 3. During these experiments, a significant portion of the total current density was generated through the OER, rather than the carbon corrosion reaction. In alkaline solutions, the OER is understood to proceed through the following 4-electron process:[92]

$$4OH^- \rightarrow O_2(g) + 2H_2O(l) + 4e^-$$

Both carbon corrosion and the OER are 4-electron processes that generate one molecule of gas-phase product, $CO_2(g)$ or $O_2(g)$ respectively. As a result, a faradaic efficiency was calculated for the IrO_2-coated GDLs based on the molar ratio of CO_2 to O_2 detected by the GC near the end of each experiment. This FE was then used as a "correction factor" for the potentiostat-based mass loss estimate.

ICP-OES was performed for IrO_2-coated and catalyst-free electrodes (Table S2†) and electrolyte solutions (Table S3†) from various corrosion experiments to characterize changes in chemical makeup resulting from carbon corrosion. Spent electrolyte solutions from corrosion tests involving IrO_2-coated electrodes did not exhibit detectable concentrations of iridium (Table S3†), suggesting that iridium did not leach into the solution at significant quantities during those corrosion tests. This is consistent with our mass loss calculations, which also did not consider any mass losses associated with dissolution of catalyst particles. ICP results also revealed that the spent electrodes contained high levels of potassium and low levels of phosphorous (Table S2†), likely caused by precipitation of the potassium phosphate electrolyte. SEM images and EDS spectra were collected for fresh and spent IrO_2-coated electrodes (Fig. S5†), but no obvious changes were seen in these samples.

Table 3 Compiled IrO_2 coated GDL mass loss estimates and measurements in phosphate electrolyte solution

					Mass loss (mg)			
Voltage (*vs.* Ag/AgCl)	Voltage (*vs.* SHE)	Corrosion time (h)	Initial electrode mass (mg)	Corrosion FE[a] (%)	Potentiostat estimate[b]	GC estimate[c]	Mass balance measurement[d]	% mass loss per day[d]
2.0	2.197	72	213.3	2.3%	4.0	3.1	3.8	0.6%
1.6	1.797	168	213.9	1.1%	2.6	2.2	2.9	0.2%

[a] Calculated based on molar ratio of $CO_2 : O_2$ detected by GC near end of experiment. [b] Estimated from the potentiostat-measured current and corrected using the calculated faradaic efficiency. [c] Estimated from the GC-measured CO_2 flowrate. [d] Reported value comes from mass balance measurements before and after corrosion experiment.

Open Access Article. Published on 31 Motsheanong 2024. Downloaded on 2024-10-01 10:24:49.
This article is licensed under a Creative Commons Attribution 3.0 Unported Licence.

This is consistent with the ICP-OES results, which showed no evidence of iridium leaching and is likely due to the small overall amount of corrosion (~2% total mass loss) that occurred during those experiments. At higher total mass loss percentages, we expect that the carbon-based MPL support would begin to disintegrate, as evidenced by SEM images of the highly corroded catalyst-free MPL (Fig. 3), resulting in significant mass losses from degradation and leaching of the catalyst layer.

4. Discussion

The mass loss results from the *ex situ* carbon corrosion test represent a significant and irreversible loss of carbon from the electrodes. For both bare GDLs and IrO_2-coated GDLs, the estimates of mass loss by both the total current passed (potentiostat estimate) and the CO_2 detected (GC estimate) closely match the actual mass loss as measured before and after each experiment (see Tables 1–3). This confirms the utility of the *ex situ* carbon corrosion test for quantifying rates of carbon corrosion in the alkaline CO_2 electrolysis environment. In operating AEM MEAs used in CO_2 electrolysis, the CO_2 produced from carbon corrosion is not able to be detected because CO_2 is present on both anode and cathode. CO_2 is fed to the cathode as a reactant, and a significant amount of CO_2 crosses over to the anode. Additionally, mass loss from carbon corrosion in AEM MEAs is very difficult to accurately measure, as the MEA must be disassembled following testing. This MEA disassembly often induces physical changes to the MEA, such as catalyst delamination. These physical changes prevent an accurate measurement of weight loss from carbon corrosion and make characterization of the spent MEA components more challenging. As such, we believe that *ex situ* corrosion tests, such as the one outlined in this manuscript, are best suited to characterizing and quantifying rates of carbon corrosion under conditions relevant to CO_2 electrolyzers.

Based on the mass loss results presented in Tables 1–3 anodic carbon corrosion is clearly a significant degradation pathway for CO_2 electrolysis systems. At an extreme anodic voltage of 2.0 V, 10% of the mass of the bare GDL is lost per day. This represents an accelerated degradation condition, as this is much higher than the anode voltage in operating MEAs. However, it is not straightforward to determine the anode voltage in operating MEAs, and most MEA tests only report cell voltage *via* a 2-electrode measurement where cell voltages around 3 V are typically reported. To determine the actual voltage experienced by the anode, membrane, and cathode in operating CO_2 MEAs, the Berlinguette group developed a cell with two reference electrodes, the first in contact with the membrane, and the second in contact with the anode GDE.[93] At 200 mA cm^{-2} and an overall cell voltage of 2.73 V, the measured voltages were −1.43, 0.71, and 0.58 V *vs.* Ag/AgCl for the cathode, membrane, and anode, respectively. To compare these results to an MEA operating with a lower pH anolyte, the potential of the OER must be corrected for pH. The OER occurs at lower potentials at higher pH, and the standard reduction potential is 0.36 V lower at pH = 14 (1 M KOH) than at pH = 8 which was used in the *ex situ* carbon corrosion test in this study. Therefore, accounting for the lower pH, the anode voltage expected when using 5 mM $KHCO_3$ as the anolyte is 0.94 V (0.58 V + 0.36 V) *vs.* Ag/AgCl. A similar study that integrated reference electrodes into operating MEAs for AEM water electrolysis reported anode voltages between 0.9 and 1.2 V *vs.* Ag/AgCl at 200 mA cm^{-2}, depending on the GDL used.[94] These results justify the use of 1 V as a realistic, or even optimistic anode voltage for operating AEM MEAs used in CO_2 electrolysis. While the corrosion mass loss is reduced at lower anodic voltages, even the relatively mild 1.0 V corrosion test (Table 1) exhibited 0.1% GDL mass loss per day. This would result in a loss of 5% of the mass of the GDL in 50 days. Similar levels of mass loss have been reported for PEMFCs, with 5% mass loss in 2000 hours (83 days) at 0.75 V.[21] Clearly, even at realistic anode voltages, carbon corrosion is too significant to lead to an acceptable MEA lifetime of at least 4 years.

Currently, a gap exists between CO_2 electrolysis anode materials employed by commercial entities and research institutions. In the literature, many studies the use of carbon-based gas diffusion media on the anode.[33–43] Contrastingly, most scale-up efforts have relied on metal-based anodes, such as Ti-based porous transport layers (PTLs). Shown in Table 4 is an overview of some industrial CO_2 electrolyzer technologies, patents, and publications with a particular focus on the design of the anode.

Early adoption of PTLs on the anode of CO_2 electrolyzers will allow for issues related to PTL-MEAs to be addressed sooner, which will ultimately lead to a quicker path to commercialization. PTL MEAs have not been sufficiently studied by the CO_2 research community, and optimization of the anode PTL for CO_2 electrolysis represents an area of impactful opportunity. Moving past the use of carbon materials on the anode for CO_2 electrolysis, there could still be corrosion concerns for the non-carbon PTLs used. While these PTLs are significantly more resistant to corrosion than carbon GDLs, the oxidative potentials experienced on the anode can still lead to durability concerns, particularly for reaching the very long lifetimes (*e.g.*, >4 years) needed for commercialization.[22,23]

Given the significant anodic carbon corrosion reported here, as well as reported carbon corrosion issues in low-temperature fuel cells and water electrolyzers, the CO_2 electrolysis community would benefit from rapidly transitioning away from the use of carbon materials on the anode. CO_2 electrolysis systems should leverage the experience in water electrolysis, as the anodic environment is similarly harsh in CO_2 electrolysis. However, it is likely that for specific short-term experiments, many in the CO_2 utilization field will continue to use carbon-based materials on the anode, as carbon GDLs have advantages including familiarity with researchers, facile mass transport of reactants and products, good electrical conductivity, low cost, and stability under mild conditions.[77] Here, we recommend that carbon materials are only appropriate on the anode for short-term experiments (<100 hours) that are not probing system durability. This follows prior recommendations from PEM water electrolysis systems, where it is not recommended to use carbon on the anode for experiments longer than 20 hours.[31] Most commercial and pilot scale CO_2 electrolyzers

 This journal is © The Royal Society of Chemistry 2024

Open Access Article. Published on 31 Motsheanong 2024. Downloaded on 2024-10-01 10:24:49.
This article is licensed under a Creative Commons Attribution 3.0 Unported Licence.

Table 4 Summarized info on industrial CO_2 electrolyzers

Company name	Target product	Electrolyzer architecture	Stack surface area (cm^2)	Conversion rate	Anode material and info
Haldor Topsoe	CO[95]	SOEC[95]	—	~4500 kg CO_2 per day (96 Nm^3 CO_2 per h)[95]	(Not a low temperature electrolyzer)
Det Norske Veritas	Formate[44]	Filter-press reactor[44]	600 (ref. 10)	1 kg CO_2 per day[10]	Ti-based with Ta_2O_5 and IrO_2 coatings[44]
Mantra Energy	Formate[45]	Trickle bed reactor[96,97]	—	100 kg CO_2 per day[10,45]	Stainless steel mesh[96]
Dioxide Materials	Formic acid[43]	MEA[43]	5 (ref. 43)	—	IrO_2 on toray paper or IrO_2 on expanded Ti[43]
	CO[48,98]	MEA[48,98]	250 (ref. 98)	—	IrO_2 on 5% carbon fiber paper[98] or Pt catalyst coated membrane[48]
Siemens and Evonik	Syngas (CO + H_2)[49,50,99]	GDE in "flow-by Mode"[99]	3000 (ref. 49 and 99)	~10 kg CO_2 per day (0.25 Nm^3 CO per hr)[99]	IrO_2 coated Ti expanded metal[50]
Liquid Light/ Avantium	Formate (to oxalic acid)[55,58]	3-Chamber configuration[58]	2000 (ref. 58)	6 kg CO_2 per day[58]	Electroless plated nickel sulfide on Cu foam[58] or Ti-based[54–57]
Twelve/Opus 12	CO[59]	MEA[60–62]	—	Few kg CO_2 per day[59]	Titanium mesh or titanium felt[60–62]

already avoid the use of carbon on the anode, due to the stability-limiting effects of carbon corrosion. Moving forward, to better align research experiments with industry best practices, CO_2 electrolysis MEA studies aimed at scale-up and commercial relevance should also move away from the utilization of carbon-based GDLs on the anode.

5. Conclusions

In this work, an *ex situ* carbon corrosion test has been developed to quantify anodic carbon corrosion in the CO_2 electrolysis environment. Using this test, extensive carbon corrosion has been quantified at realistic anodic voltages experienced in operating CO_2 electrolysis cells. The mass loss from carbon corrosion measured in the *ex situ* experiments was found to closely match mass loss estimates from both the total CO_2 detected from the experiment and from the total current passed. An unacceptably high mass loss has been quantified for both IrO_2-coated and catalyst-free carbon GDLs. Given the carbon corrosion results presented here and following guidance from scaled-up industrial CO_2 electrolyzers, we recommend that the field moves away from using carbon-based materials on the anode of CO_2 MEAs. If carbon materials are employed on the anode of CO_2 electrolysis systems, it is only appropriate for short-term experiments at low cell voltages. However, for longer-term experiments (>100 hours) and experiments investigating durability of CO_2 MEAs, carbon-based anodes should be avoided entirely.

Author contributions

J. Ferrell: conceptualization, investigation, formal analysis, writing – original draft, writing – review & editing, supervision, funding acquisition, project administration. M. Rasmussen: investigation, formal analysis, writing – original draft, writing – review & editing. W. W. McNeary: investigation, writing – review & editing.

Conflicts of interest

There are no conflicts to declare.

Acknowledgements

This work was authored by the National Renewable Energy Laboratory, operated by Alliance for Sustainable Energy, LLC, for the U. S. Department of Energy (DOE) under Contract No. DE-AC36-08GO28308. Funding provided by the U. S. Department of Energy Office of Energy Efficiency and Renewable Energy Bioenergy Technologies Office. The views expressed in the article do not necessarily represent the views of the DOE or the U. S. Government. The U. S. Government retains and the publisher, by accepting the article for publication, acknowledges that the U. S. Government retains a nonexclusive, paid-up, irrevocable, worldwide license to publish or reproduce the published form of this work, or allow others to do so, for U. S. Government purposes.

Notes and references

1 *AR6 Synthesis Report: Climate Change 2023*, 2023.
2 S. J. Davis, N. S. Lewis, M. Shaner, S. Aggarwal, D. Arent, I. L. Azevedo, S. M. Benson, T. Bradley, J. Brouwer, Y. M. Chiang, C. T. M. Clack, A. Cohen, S. Doig, J. Edmonds, P. Fennell, C. B. Field, B. Hannegan, B. M. Hodge, M. I. Hoffert, E. Ingersoll, P. Jaramillo, K. S. Lackner, K. J. Mach, M. Mastrandrea, J. Ogden, P. F. Peterson, D. L. Sanchez, D. Sperling, J. Stagner, J. E. Trancik, C. J. Yang, K. Caldeira, *et al.*, *Science*, 2018, **360**(6396), eaas9793.

Open Access Article. Published on 31 Motsheanong 2024. Downloaded on 2024-10-01 10:24:49.
This article is licensed under a Creative Commons Attribution 3.0 Unported Licence.

3 R. G. Grim, D. Ravikumar, E. C. D. Tan, Z. Huang, J. R. Ferrell, M. Resch, Z. Li, C. Mevawala, S. D. Phillips, L. Snowden-Swan, L. Tao and J. A. Schaidle, *Energy Environ. Sci.*, 2022, **15**, 4798–4812.
4 *2016 Billion-Ton Report: Advancing Domestic Resources for a Thriving Bioeconomy*, 2016.
5 R. G. Grim, Z. Huang, M. T. Guarnieri, J. R. Ferrell, L. Tao and J. A. Schaidle, *Energy Environ. Sci.*, 2020, **13**, 472–494.
6 H. Shin, K. U. Hansen and F. Jiao, *Nat. Sustain.*, 2021, **4**, 911–919.
7 Z. Huang, R. G. Grim, J. A. Schaidle and L. Tao, *Energy Environ. Sci.*, 2021, **14**, 3664–3678.
8 M. Goldman, A. Prajapati, E. Duoss, S. Baker and C. Hahn, *Curr. Opin. Electrochem.*, 2023, **39**, 101248.
9 B. Endrődi, G. Bencsik, F. Darvas, R. Jones, K. Rajeshwar and C. Janáky, *Prog. Energy Combust. Sci.*, 2017, **62**, 133–154.
10 O. G. Sánchez, Y. Y. Birdja, M. Bulut, J. Vaes, T. Breugelmans and D. Pant, *Curr. Opin. Green Sustainable Chem.*, 2019, **16**, 47–56.
11 S. D. Ebbesen and M. Mogensen, *J. Power Sources*, 2009, **193**, 349–358.
12 Y. Song, X. Zhang, K. Xie, G. Wang and X. Bao, *Adv. Mater.*, 2019, **31**, 1902033.
13 D. Higgins, C. Hahn, C. Xiang, T. F. Jaramillo and A. Z. Weber, *ACS Energy Lett.*, 2019, **4**, 317–324.
14 E. W. Lees, B. A. W. Mowbray, F. G. L. Parlane and C. P. Berlinguette, *Nat. Rev. Mater.*, 2021, **7**, 55–64.
15 D. T. Whipple, E. C. Finke and P. J. A. Kenis, *Electrochem. Solid-State Lett.*, 2010, **13**, B109–B111.
16 L. Ge, H. Rabiee, M. Li, S. Subramanian, Y. Zheng, J. H. Lee, T. Burdyny and H. Wang, *Chem*, 2022, **8**, 663–692.
17 I. Merino-Garcia, E. Alvarez-Guerra, J. Albo and A. Irabien, *Chem. Eng. J.*, 2016, **305**, 104–120.
18 U. O. Nwabara, M. P. De Heer, E. R. Cofell, S. Verma, E. Negro and P. J. A. Kenis, *J. Mater. Chem. A*, 2020, **8**, 22557–22571.
19 S. Verma, B. Kim, H. R. M. Jhong, S. Ma and P. J. A. Kenis, *ChemSusChem*, 2016, **9**, 1972–1979.
20 R. G. Grim, J. R. Ferrell, Z. Huang, L. Tao and M. G. Resch, *Joule*, 2023, **7**, 1684–1699.
21 U. O. Nwabara, E. R. Cofell, S. Verma, E. Negro and P. J. A. Kenis, *ChemSusChem*, 2020, **13**, 855–875.
22 T. Labi, F. Van Schalkwyk, S. M. Andersen, P. Morgen, S. C. Ray and J. Chamier, *J. Power Sources*, 2021, **490**, 229568.
23 T. R. Ralph, S. Hudson and D. P. Wilkinson, *ECS Trans.*, 2006, **1**, 67–84.
24 N. Garland, T. Benjamin and J. Kopasz, *ECS Trans.*, 2007, **11**, 923–931.
25 T. Abdel-Baset, T. Benjamin, R. Borup, K. Epping Martin, N. Garland, S. Hirano, J. Kopasz, B. Lakshmanan, D. Masten, M. Mehall, D. Myers, D. Papageorgopoulos, W. Podolski, T. Trabold, B. Vermeersch and J. Waldecker, *Fuel Cell Technical Team Roadmap*, 2013.
26 P. Ren, P. Pei, Y. Li, Z. Wu, D. Chen and S. Huang, *Prog. Energy Combust. Sci.*, 2020, **80**, 100859.
27 J. Sim, M. Kang, K. Min, E. Lee and J. Y. Jyoung, *Renew. Energy*, 2022, **190**, 959–970.
28 T. Ha, J. Cho, J. Park, K. Min, H. S. Kim, E. Lee and J. Y. Jyoung, *Int. J. Hydrogen Energy*, 2011, **36**, 12436–12443.
29 K. Tomantschger, R. Findlay, M. Hanson, K. Kordesch and S. Srinivasan, *J. Power Sources*, 1992, **39**, 21–41.
30 K. Ayers, N. Danilovic, R. Ouimet, M. Carmo, B. Pivovar and M. Bornstein, *Annu. Rev. Chem. Biomol. Eng.*, 2019, **10**, 219–239.
31 G. Bender, M. Carmo, T. Smolinka, A. Gago, N. Danilovic, M. Mueller, F. Ganci, A. Fallisch, P. Lettenmeier, K. A. Friedrich, K. Ayers, B. Pivovar, J. Mergel and D. Stolten, *Int. J. Hydrogen Energy*, 2019, **44**, 9174–9187.
32 Z. Kang, S. M. Alia, J. L. Young and G. Bender, *Electrochim. Acta*, 2020, **354**, 136641.
33 U. O. Nwabara, A. D. Hernandez, D. A. Henckel, X. Chen, E. R. Cofell, M. P. De-Heer, S. Verma, A. A. Gewirth and P. J. A. Kenis, *ACS Appl. Energy Mater.*, 2021, **4**, 5175–5186.
34 R. B. Kutz, Q. Chen, H. Yang, S. D. Sajjad, Z. Liu and I. R. Masel, *Energy Technol.*, 2017, **5**, 929–936.
35 S. Hernandez-Aldave and E. Andreoli, *Catalysts*, 2020, **10**, 713.
36 Z. Liu, H. Yang, R. Kutz and R. I. Masel, *J. Electrochem. Soc.*, 2018, **165**, J3371–J3377.
37 B. Endrődi, E. Kecsenovity, A. Samu, F. Darvas, R. V. Jones, V. Török, A. Danyi and C. Janáky, *ACS Energy Lett.*, 2019, **4**, 1770–1777.
38 K. Jiang, S. Siahrostami, T. Zheng, Y. Hu, S. Hwang, E. Stavitski, Y. Peng, J. Dynes, M. Gangisetty, D. Su, K. Attenkofer and H. Wang, *Energy Environ. Sci.*, 2018, **11**, 893–903.
39 L. M. Aeshala, R. Uppaluri and A. Verma, *Phys. Chem. Chem. Phys.*, 2014, **16**, 17588–17594.
40 R. L. MacHunda, J. Lee and J. Lee, *Surf. Interface Anal.*, 2010, **42**, 564–567.
41 Z. Bitar, A. Fecant, E. Trela-Baudot, S. Chardon-Noblat and D. Pasquier, *Appl. Catal., B*, 2016, **189**, 172–180.
42 S. Lee, H. K. Ju, R. Machunda, S. Uhm, J. K. Lee, H. J. Lee and J. Lee, *J. Mater. Chem. A*, 2015, **3**, 3029–3034.
43 H. Yang, J. J. Kaczur, S. D. Sajjad and R. I. Masel, *J. CO_2 Util.*, 2017, **20**, 208–217.
44 Y. Zhai, S. Guan, N. Sridhar and A. Agarwal, Method and Apparatus for the Electrochemical Reduction of Carbon Dioxide, WO2012040503A2, 2012.
45 P. Ganji, R. A. Borse, J. Xie, A. G. A. Mohamed and Y. Wang, *Adv. Sustainable Syst.*, 2020, **4**, 2000096.
46 C. Oloman and H. Li, Continuous Co-Current Electrochemical Reduction Of Carbon Doxde, *US Pat.*, US20160068974A1, 2016.
47 J. J. Kaczur, H. Yang, S. D. Sajjad and R. I. Masel, Method And System For Electrochemical Production Of Formic Acid From Carbon Dioxide, *US Pat.*, US10047446B2, 2018.
48 R. I. Masel, B. A. Rosen and W. Zhu, Devices And Processes For Carbon Doxde Conversion Into Useful Fuels And Chemicals, *US Pat.*, US9181625B2, 2015.
49 CO2 for a clean performance: Rheticus research project enters phase 2, **https://press.siemens.com/global/en/pressrelease/research-project-rheticus**, accessed 19 August 2023.

 This journal is © The Royal Society of Chemistry 2024

Open Access Article. Published on 31 Motsheanong 2024. Downloaded on 2024-10-01 10:24:49.
This article is licensed under a Creative Commons Attribution 3.0 Unported Licence.

50 R. Krause, D. Reinisch, C. Reller, H. Eckert, D. Hartmann, D. Taroata, K. Wiesner-Fleischer, A. Bulan, A. Lueken and G. Schmid, *Chem. Ing. Tech.*, 2020, **92**, 53–61.
51 T. Haas, R. Krause, R. Weber, M. Demler and G. Schmid, *Nat. Catal.*, 2018, **1**, 32–39.
52 R. Krause, C. Reller, G. Schmid, B. Schmid and F. Steinbacher, Production Of Gas Diffusion Electrodes Comprising Ion Transport Resins For Electrochemical Reduction Of CO_2, *US Pat.*, US20200131649A1, 2020.
53 B. Schmid, C. Reller and G. Schmid, Two-Membrane Construction For Electrochemically Reducing CO, *US Pat.*, US20200080211A1, 2020.
54 J. J Kaczur, P. Kaczur and K. Teamey, Method And System For Electrochemical Reduction Of Carbon Dioxide Employing A Gas Diffusion Electrode, *US Pat.*, US10329676, 2019.
55 J. J. Kaczur and K. Teamey, Integrated Process For Producing Carboxylic Acids From Carbon Doxde, *US Pat.*, US9085827B2, 2015.
56 J. J. Kaczur, P. Lakkaraju and J. Krasovic, Method and System for Electrochemical Reduction of Carbon Dioxide Employing a Gas, WO2017118712A1, 2017.
57 Z. Twardowski, E. B. Cole, J. J. Kaczur, K. Teamey, K. A. Keets, R. Parajuli, A. Bauer, N. Sivasankar, G. Leonard, T. J. Kramer, P. Majsztrik and Y. Zhu, Method and System for Production of Oxalic Acid and Oxalic Acid Reduction Products, *US Pat.*, US9267212B2, 2016.
58 P. Moser, S. Schmidt, K. Stahl, A. Mol, D. Petrutiu, J. Krasovic, A. Smith, A. Turetta, A. Morosanu and M. Antonini, in *16th International Conference on Greenhouse Gas Control Technologies (GHGT-16)*, SSRN, 2022, DOI: **10.2139/SSRN.4274076**.
59 A. K. Buckley, S. Ma, Z. Huo, T. Z. Gao and K. P. Kuhl, *Nat. Nanotechnol.*, 2022, **17**, 811–813.
60 K. P. Kuhl, E. R. Cave and G. Leonard, Reactor With Advanced Architecture For The Electrochemical Reaction Of CO_2, CO, And Other Chemical Compounds, *US Pat.*, US20220010437A1, 2022.
61 E. R. Cave, S. Ma, Q. Zeng, S. Hunegnaw, K. P. Kuhl, G. Leonard, A. D. Mishra and A. R. Kashi, George Leonard, Ashley D. Mishra, Ajay R. Kashi, Electrolyzer and Method of Use, *US Pat.*, US20230136397A1, 2023.
62 E. P. Kuhl, E. R. Cave and G. Leonard, Reactor With Advanced Architecture For The Electrochemical Reaction Of CO_2, CO, And Other Chemical Compounds, *US Pat.*, US20210395908A1, 2021.
63 S. Hunegnaw, A. R. Kashi, K. P. Kuhl, M. George, S. Ma, Z. Huo, E. R. Cave and K. X. Hua, System And Method For Methane Production, *US Pat.*, US20200216968A1, 2020.
64 United States Department of Energy, Energy Efficiency and Renewable Energy, Fuel Cell Technologies OfficeMulti-Year Research, Development, and Demonstration Plan Planned program activities for 2011–2020, ch. 3.4: Fuel Cells, **https://www.energy.gov/sites/prod/files/2014/12/f19/fcto_myrdd_full_document.pdf**.
65 G. Tsotridis and A. Pilenga, *EU Harmonised Protocols for Testing of Low Temperature Water Electrolysers*, 2021.
66 J. R. Varcoe, P. Atanassov, D. R. Dekel, A. M. Herring, M. A. Hickner, P. A. Kohl, A. R. Kucernak, W. E. Mustain, K. Nijmeijer, K. Scott, T. Xu and L. Zhuang, *Energy Environ. Sci.*, 2014, **7**, 3135–3191.
67 S. G. Ji, H. Kim, W. H. Lee, H. S. Oh and C. H. Choi, *J. Mater. Chem. A*, 2021, **9**, 19834–19839.
68 S. Maass, F. Finsterwalder, G. Frank, R. Hartmann and C. Merten, *J. Power Sources*, 2008, **176**, 444–451.
69 S. Möller, S. Barwe, J. Masa, D. Wintrich, S. Seisel, H. Baltruschat and W. Schuhmann, *Angew. Chem., Int. Ed.*, 2020, **59**, 1585–1589.
70 A. A. Samu, I. Szenti, Á. Kukovecz, B. Endrődi and C. Janáky, *Commun. Chem.*, 2023, **6**, 1–9.
71 Y. Wu, S. Garg, M. Li, M. N. Idros, Z. Li, R. Lin, J. Chen, G. Wang and T. E. Rufford, *J. Power Sources*, 2022, **522**, 230998.
72 N. Schwartz, J. Harrington, K. J. Ziegler and P. Cox, *ACS Omega*, 2022, **7**, 29832–29839.
73 B. J. M. Etzold, U. Krewer, S. Thiele, A. Dreizler, E. Klemm and T. Turek, *Chem. Eng. J.*, 2021, **424**, 130501.
74 S. A. Grigoriev, P. Millet, S. A. Volobuev and V. N. Fateev, *Int. J. Hydrogen Energy*, 2009, **34**, 4968–4973.
75 C. H. Lee, R. Banerjee, F. Arbabi, J. Hinebaugh and A. Bazylak, in *ASME 2016 14th International Conference on Nanochannels, Microchannels, and Minichannels (ICNMM2016)*, American Society of Mechanical Engineers Digital Collection, 2016.
76 T. Schuler, R. De Bruycker, T. J. Schmidt and F. N. Büchi, *J. Electrochem. Soc.*, 2019, **166**, F270–F281.
77 T. L. Doan, H. E. Lee, S. S. H. Shah, M. J. Kim, C. H. Kim, H. S. Cho and T. Kim, *Int. J. Energy Res.*, 2021, **45**, 14207–14220.
78 S. Stiber, N. Sata, T. Morawietz, S. A. Ansar, T. Jahnke, J. K. Lee, A. Bazylak, A. Fallisch, A. S. Gago and K. A. Friedrich, *Energy Environ. Sci.*, 2022, **15**, 109–122.
79 F. J. Pérez-Alonso, C. Adán, S. Rojas, M. A. Peña and J. L. G. Fierro, *Int. J. Hydrogen Energy*, 2014, **39**, 5204–5212.
80 N. K. Chaudhari, H. Jin, B. Kim and K. Lee, *Nanoscale*, 2017, **9**, 12231–12247.
81 J. E. Park, H. J. Choi, S. Y. Kang, G. Y. Jang, O. H. Kim, M. Karuppannan, Y. E. Sung, O. J. Kwon and Y. H. Cho, *Int. J. Energy Res.*, 2022, **46**, 16670–16678.
82 T. Schuler, R. De Bruycker, T. J. Schmidt and F. N. Büchi, *J. Electrochem. Soc.*, 2017, **166**, F270.
83 C. C. L. McCrory, S. Jung, J. C. Peters and T. F. Jaramillo, *J. Am. Chem. Soc.*, 2013, **135**, 16977–16987.
84 T. Reier, M. Oezaslan and P. Strasser, *ACS Catal.*, 2012, **2**, 1765–1772.
85 K. Jiao, J. Xuan, Q. Du, Z. Bao, B. Xie, B. Wang, Y. Zhao, L. Fan, H. Wang, Z. Hou, S. Huo, N. P. Brandon, Y. Yin and M. D. Guiver, *Nature*, 2021, **595**, 361–369.
86 I. Jang, I. Hwang and Y. Tak, *Electrochim. Acta*, 2013, **90**, 148–156.
87 Y. Wang, C. Zhou, X. Xie, C. Yang, Q. Feng, J. Zou, X. Z. Yuan, J. Fan, L. Zeng, H. Li and H. Wang, *Int. J. Hydrogen Energy*, 2020, **45**, 996–1007.
88 H. E. Kim, S. Shin and H. Lee, *J. Catal.*, 2021, **395**, 404–411.

Open Access Article. Published on 31 Motsheanong 2024. Downloaded on 2024-10-01 10:24:49.
This article is licensed under a Creative Commons Attribution 3.0 Unported Licence.

89 F. Maillard, A. Bonnefont and F. Micoud, *Electrochem. Commun.*, 2011, **13**, 1109–1111.
90 L. M. Roen, C. H. Paik and T. D. Jarvi, *Electrochem. Solid-State Lett.*, 2004, **7**, A19.
91 J. Willsau and J. Heitbaum, *J. Electroanal. Chem. Interfacial Electrochem.*, 1984, **161**, 93–101.
92 B. Zhang, N. Wang, T. Dwi Widodo, R. Raharjo, R. Bintarto, Q. Liang, G. Brocks and A. Bieberle-Hütter, *J. Phys.: Energy*, 2021, **3**, 026001.
93 D. Salvatore and C. P. Berlinguette, *ACS Energy Lett.*, 2020, **5**, 215–220.
94 Q. Xu, S. Z. Oener, G. Lindquist, H. Jiang, C. Li and S. W. Boettcher, *ACS Energy Lett.*, 2021, **6**, 2238–2239.
95 R. Küngas, P. Blennow, T. Heiredal-Clausen, T. Holt, J. Rass-Hansen, S. Primdahl and J. B. Hansen, *ECS Trans.*, 2017, **78**, 2879–2884.
96 R. Gilliam, T. A. Albrecht, N. Jalani, N. A. Knott, V. Decker, M. Kostowsky, B. Boggs, A. Gorer and K. Farsad, Electrochemical System And Method For CO_2 Utilization, 2007.
97 C. W. Oloman and A. P. Watkinson, Electrochemical System And Method For CO_2 Utilization, Electrolytic Production Of Alkaline Peroxide Solutions, *US Pat.*, US3969201, 1976.
98 J. J. Kaczur, H. Yang, Z. Liu, S. D. Sajjad and R. I. Masel, *Front. Chem.*, 2018, **6**, 377597.
99 G. Schmid, N. Martic, R. Krause, C. Reller, H. Eckert, K. Wiesner-Fleischer, H. Neubert, S. Energy, T. Haas, M. Demmler, L. Reinicke and A. Hecker, The Rheticus Project (Technical/Artificial Photosynthesis) Renewable Synthesis of chemical Feedstock and Specialties employing Electrolysis & Syngas Fermentation, Surfcat, *Surfcat Summer School: The Science of Sustainable Fuels and Chemicals*, Gilleleje, Denmark, 2022.

 This journal is © The Royal Society of Chemistry 2024